Lift induced by slip inhomogeneities in lubricated contacts

Aidan Rinehart, Uğis Lācis, Thomas Salez, Shervin Bagheri

▶ **To cite this version:**

Lift induced by slip inhomogeneities in lubricated contacts

Aidan Rinehart[1], Uğis Lācis[1], Thomas Salez[2], and Shervin Bagheri[1]*

[1] Dept. Mechanics, KTH Royal Institute of Technology, Stockholm 11428, SE and
[2] Univ. Bordeaux, CNRS, LOMA, UMR 5798, F-33405, Talence, France

Lubrication forces depend to a high degree on elasticity, texture, charge, chemistry, and temperature of the interacting surfaces. Therefore, by appropriately designing surface properties, we may tailor lubrication forces to reduce friction, adhesion and wear between sliding surfaces or control assembly, repulsion, and collision of interacting particles. Here, we show that variations of slippage on one of the contacting surfaces induce a normal (lift) force. We demonstrate the consequences of this force on the mobility of a cylinder traveling near a wall and show the emergence of active-like particle trajectories, such as oscillation, migration, and propulsion. Our study has implications for understanding how inhomogeneous biological interfaces interact with their environment; it also reveals a new method of patterning surfaces for controlling the motion of nearby particles.

In many physical processes, the flow of small particles such as cells, colloids, bubbles, grains, and fibers occurs near soft, porous and rough walls. The induced lubrication forces [1] on these particles depend on the elasticity, texture, and chemistry of the nearby wall. These hydrodynamic forces may very well dominate over both bulk (e.g. Stokes drag) and surface (e.g. van der Waals and electrostatic) forces, and therefore determine single-particle motion and collective behavior.

The simplest configuration to characterize hydrodynamic particle-wall forces is that of an infinitely long circular cylinder traveling parallel to a rigid flat wall. At low Reynolds numbers, the cylinder will experience zero wall-normal (lift) force and therefore move at a constant distance from the wall [2]. This is due to the time-reversal symmetry of the Stokes equations. However, when the rigid wall is replaced with a soft surface, the moving particle is repelled from the wall [3] as a result of the broken symmetry of the fluid pressure in the thin gap [4, 5]. This elastohydrodynamic lift mechanism increases the gap thickness and thus reduces wear and friction between the siding surfaces [6]. It underlies exotic particle trajectories such as oscillations, Magnus-like effect, stick-slip motion, and spinning [7, 8]. Soft lubrication also underpins the principle of surface rheology [9, 10] that is used to characterize the viscoelasticity of complex surfaces.

Besides softness, another ubiquitous feature of surfaces in biological and technological applications is surface inhomogeneities. For example, the surface of a Janus particle is divided into two halves with different chemistry (hydrophobic/hydrophilic) or texture (rough/smooth). This provides the particle with unique capabilities including self-assembly into complex structures [11] and self-propulsion [12]. More generally, interfaces in living tissues (cell walls, blood vessels, cartilage, epithelia, etc.) vary in chemical and mechanical composition due to inhomogenous distribution of cells and proteins. In technological applications, inhomogenous surfaces arise as con-

sequence of manufacturing imperfections and wear, but also from surface patterning to control liquid transport [13] or heat transfer [14]. Despite this ubiquity, there has been no investigation of the full set of lubrication forces arising from particle-wall interaction when the properties of one of the contacting surfaces vary.

In this Letter, we study lubrication forces when slippage [15] properties change along the contacting surfaces. We consider a minimal model of spatially varying slip length ℓ at either the surface of a flat wall or at the surface of a cylinder (Fig. 1a,b). Here, ℓ is defined as an effective material property of an interface at some coarse-grained level. The slip length can therefore be considered as a mesoscopic model emerging from small-scale features such as surface charges [16], wall roughness [17], super-hydrophobicity [18], liquid infusion [19], and temperature or solute concentration gradients [20].

Using analytical and numerical treatments, we demonstrate that surface inhomogeneities give rise to particle trajectories such as oscillations, migration and propulsion. Underlying these phenomena is the generation of a normal lift force that arises from spatial variations in surface slippage. To illustrate this, consider the two configurations shown in Fig. 1(c,d). Both cases involve a cylinder of radius r located a distance δ_0 from a flat wall and immersed in a fluid with viscosity η and density ρ. We assume small Reynolds number, $Re = \rho V r/\eta \ll 1$, where V is the characteristic velocity of the cylinder.

Figure 1(e) (blue line) shows the trajectory of the cylinder falling freely under gravity next to a wall that has a single slip transition. The trajectory is obtained from numerical simulations of Stokes equations coupled to Newton's equation of motion for the cylinder (see SI). As the cylinder passes the transition line, it migrates away from the wall a distance Δ, that is comparable to δ_0. In contrast, a wall with homogeneous slippage produces zero wall-normal lift force (and consequently no wall-normal motion) on a cylinder [21]. Therefore, the lift arises here from the sudden change in slip length at the wall. By carrying out an expansion in the dimensionless slip length $L = \ell/\delta_0$, we will show below that the lift force per

---
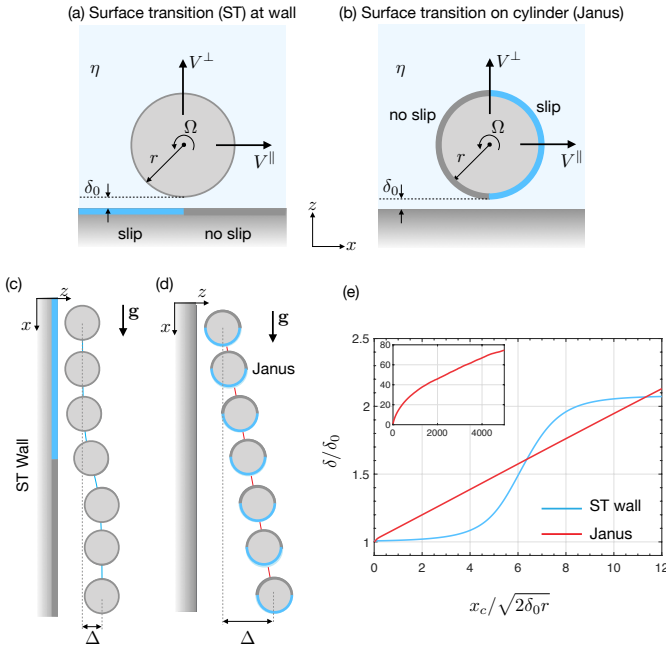* corresponding author: shervin@mech.kth.se

FIG. 1. The two lubrication models considered. (a) 2D solid cylinder moving near a flat wall with a transition from a slip (blue) to a no slip (grey). (b) 2D cylinder half-coated with a slip region and moving near a wall. (c),(d) Sketches of cylinder trajectories for the two systems placed in a gravity field with initial gap size $\delta_0 = 0.05r$, slip length $\ell = 1.79\delta_0$ and cylinder density $\rho_c = 10\rho$. (e) Normalized gap thickness versus the transverse displacement of the cylinder. The latter is normalized by the length of the contact zone $l_c = \sqrt{2\delta_0 r}$, where lubrication forces are important. Inset shows the trajectory of the Janus cylinder over a large spatial extent.

unit length of the cylinder scales at the lowest order as $F_z \sim \eta V^{\parallel}\varepsilon^{-1}L$ at the transition line, and that $\Delta \sim \ell$, where $\varepsilon = \delta_0/r \ll 1$ is the initial lubrication parameter. Importantly, this new lift force can be comparable in magnitude to other lubrication forces. For example, for a red blood cell traveling near glycocalyx [22], variations of the slip length as small as a few nanometers induce a lift force comparable to the elastohydrodynamic one (~ 0.1 pN) caused by glycocalyx deformation [23].

Figure 1(e) (red line) shows the trajectory (obtained from numerical simulations) of a Janus cylinder falling freely under gravity near a flat wall (Fig. 1d). In contrast to the previous model system, we observe a persistent normal drift along the trajectory, since the transition from slip to no-slip is now located on the traveling cylinder itself thus constantly inducing a wall-normal force. Scaling estimates, that will be obtained below at lowest order in L, indicate that $\Delta \sim x_c \ell/l_c$, where $l_c = \sqrt{2\delta_0 r}$ is the lubrication contact length and x_c is the transverse displacement. As Δ becomes comparable to and larger than r, one expects eventually a saturation of normal migration, since lubrication forces become negligible in the bulk. Nevertheless, as shown in the inset of Fig. 1(e), the effect holds even for δ substantially larger than r.
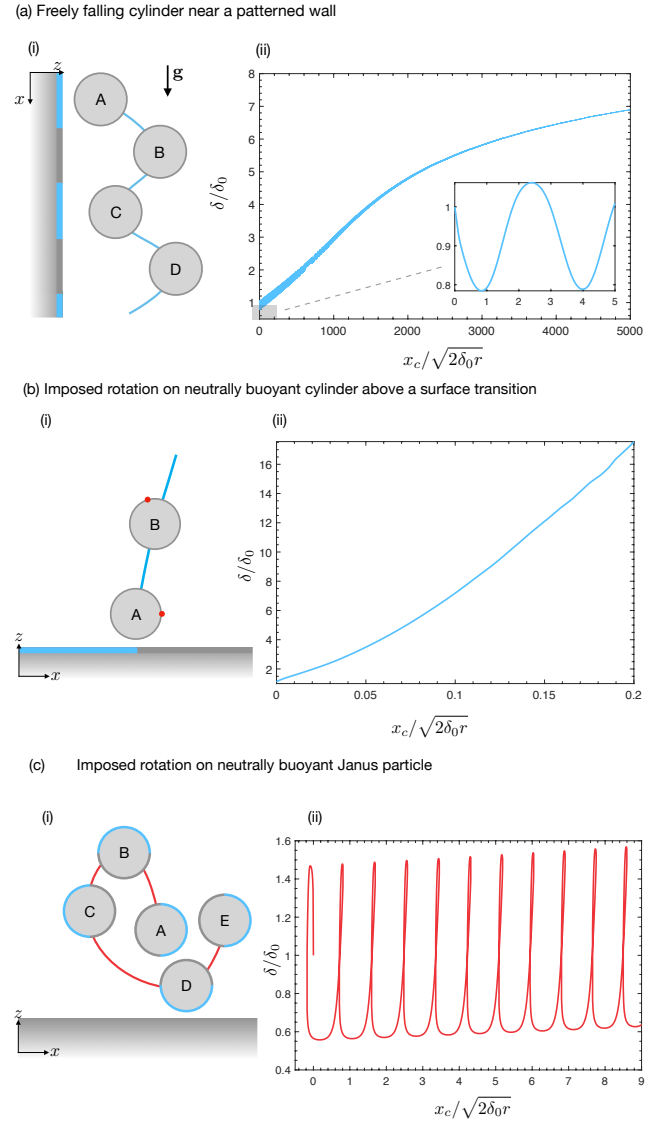

FIG. 2. Cylinder trajectories induced by variation of slippage. (a) Cylinder falling under gravity near a wall that alternates between slip (blue) and no slip (grey). (b) Neutrally buoyant cylinder rotating at fixed angular speed and initially centered above a single slip-to-no-slip transition on the wall. (c) Neutrally buoyant Janus cylinder rotating at fixed angular speed next to a wall. Right column (ii) shows the evolution of the normalized gap thickness as a function of the normalized transverse displacement of the cylinder. For all configurations, $\delta_0/r = 0.05$ and $L = 1.79$.

The intimate coupling of rigid-body motion to slippage inhomogeneities can result in unexpected particle dynamics. Examples are shown in Fig. 2, and include oscillatory motion of a cylinder translating near a wall that alternates between slip and no slip (Fig. 2a); drift and translation of a rotating cylinder above a single slip to no-slip transition (Fig. 2b); and spiralling propulsive motion of a rotating Janus cylinder next to a wall (Fig. 2c). In the remainder of this Letter, we will study in detail these motions using lubrication theory and scaling laws.
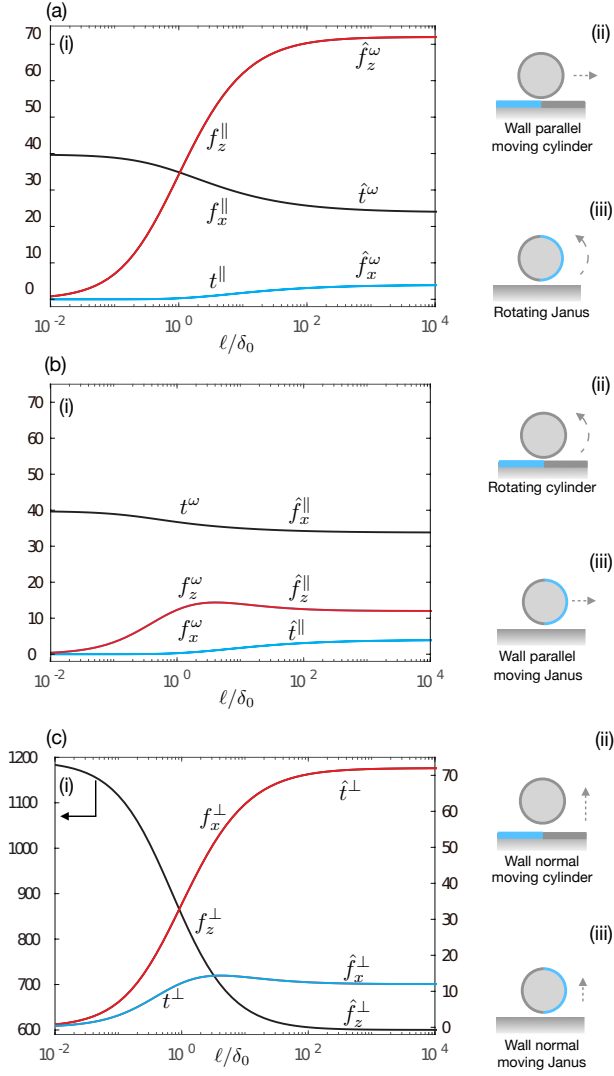
FIG. 3. Left frame shows analytic solutions of resistance co-
efficients in (1) for both model systems. The coefficients cor-
respond to the configurations shown in the right frame. The
gray dashed arrow indicates the imposed motion. Results are
for $\varepsilon = 0.05$, which corresponds to the value used in the nu-
merical solutions.

At low Reynolds numbers, the hydrodynamic force per
unit length, $\mathbf{F} = (F_x, F_z)$, and torque per unit length, T,
acting on the cylinder are linearly related to the velocity
$\mathbf{V} = (V^\parallel, V^\perp)$ and the angular speed Ω of the cylinder.
This is expressed by the symmetric resistance matrix [24],

$$\begin{bmatrix} F_x \\ F_z \\ T \end{bmatrix} = -\eta \begin{bmatrix} f_x^\parallel & -f_x^\perp & rf_x^\omega \\ -f_z^\parallel & f_z^\perp & -rf_z^\omega \\ rt^\parallel & -rt^\perp & r^2t^\omega \end{bmatrix} \begin{bmatrix} V^\parallel \\ V^\perp \\ \Omega \end{bmatrix}, \quad (1)$$

where $f_x^\perp = f_z^\parallel$, $t^\parallel = f_x^\omega$ and $t^\perp = f_z^\omega$. Assuming a small
gap between the surfaces, $\varepsilon = \delta_0/r \ll 1$, we here explain
the procedure to determine the elements of the resistance
matrix for the cylinder translating parallel to the wall
with a sudden slip-to-no-slip transition (Fig. 3a,ii). The
other matrix elements are obtained in an analogous way.

We non-dimensionalize the variables as,

$$x = l_c X, \qquad z = \delta_0 Z, \qquad h = \delta_0 H,$$
$$u = V^\parallel U, \qquad w = \frac{\varepsilon^{1/2}V^\parallel}{\sqrt{2}} W, \qquad p = \frac{l_c \eta V^\parallel}{\delta_0^2} P,$$

where, u, w are, respectively, the transverse and normal
components of the fluid velocity, p is the fluid excess pres-
sure with respect to the atmospheric one. The cylinder
surface is approximated at one instant in time, shown in
Fig. 1(a), as $h(x) = \delta_0 + x^2/(2r)$. Inserting the dimen-
sionless variables into the continuity and Stokes equa-
tions and neglecting $\mathcal{O}(\varepsilon)$ terms, we obtain

$$\partial_X P = \partial_{ZZ} U, \quad \partial_Z P = 0, \quad \partial_X U + \partial_Z W = 0. \quad (2)$$

In the laboratory frame of reference, where the wall is
at rest, the boundary conditions are,

$$W|_{Z=0,H} = 0, \qquad U|_{Z=H} = 1, \quad (3)$$
$$U|_{Z=0} = L\partial_Z U|_{Z=0} S. \quad (4)$$

The third condition accounts for slippage and is modelled
through a Navier boundary condition. Moreover, S is a
step function that equals one for $X < 0$ and zero for
$X > 0$, where $X = 0$ is the location on the wall of the
transition from slip to no slip. The solution of (2) and
(4) is a combination of Couette and Poiseuille flows (see
SI). From that solution, the fluid stress is projected onto
the cylinder surface to obtain the elements in (1), i.e.

$$f_x^\parallel = \sqrt{2}\varepsilon^{-1/2} \int_{-\infty}^\infty (2XP + \partial_Z U)\, dX, \quad (5)$$

$$f_z^\parallel = 2\varepsilon^{-1} \int_{-\infty}^\infty P dX, \quad (6)$$

$$t^\parallel = \sqrt{2}\varepsilon^{-1/2} \int_{-\infty}^\infty \partial_Z U dX. \quad (7)$$

Figure 3(a,i) shows the elements (5-7) of the resistance
matrix as a function of dimensionless slip length. When
$\ell/\delta_0 \to 0$, only the drag coefficient ($f_x^\parallel$) is non-zero, in
agreement with the results for no slip surfaces [2]. When
$\ell \approx \delta_0$ and for larger ℓ, we note the emergence of non-
zero elements related to lift force ($f_z^\parallel$) (as reported nu-
merically in Fig. 1e) and torque $t^\parallel$.

Figure 3(b,i) shows the elements (denoted by theˆsym-
bol) induced by a Janus cylinder that translates parallel
to a wall. We again observe the emergence of off-diagonal
terms of the resistance matrix for $\ell \approx \delta_0$; in particular
the lift force ($\hat{f}_z^\parallel$) that is responsible for the constant
normal migration shown in Fig. 1(e) (red). The com-
plete set of elements for both model systems is reported
in Fig. 3. Note that due to the Lorentz reciprocal theo-
rem [24] there is a deep symmetry between the two model
systems.

To understand in more detail the lift-inducing mecha-
nism of slip-to-no-slip transitions, we study the gap pres-
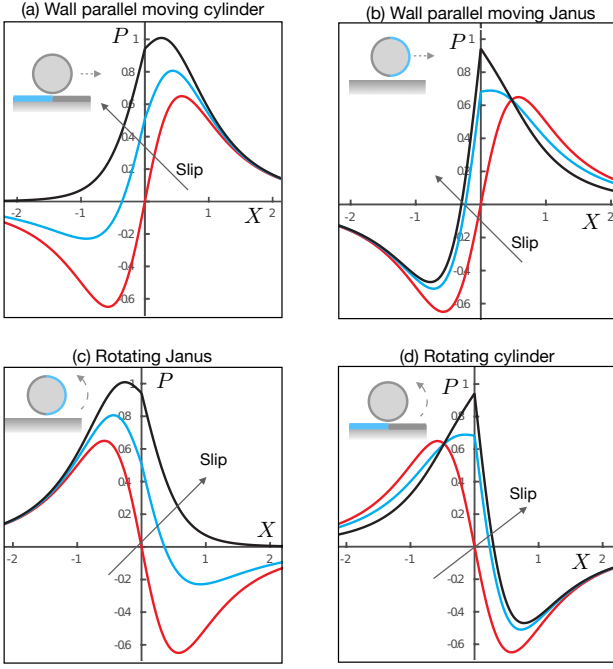sure distributions for three different slip lengths. Figure

FIG. 4. Lift generating lubrication pressure distributions for three different slip lengths. Imposed slip lengths are $L = 0$ (red), $L = 1$ (blue) and $L = \infty$ (black).

TABLE I. Scaling laws for lift force (F_z) and wall-normal displacement (Δ) for ST Wall or Janus particle. The imposed motion is either wall-parallel velocity or rotation. For the latter, the displacement shown is for one revolution.

	Motion	Lift force	Displacement
ST Wall	$V^{\parallel}$	$F_z \sim \eta V^{\parallel} \varepsilon^{-1} L$	$\Delta \sim \ell$
Janus	$V^{\parallel}$	$F_z \sim \eta V^{\parallel} \varepsilon^{-1} L$	$\Delta \sim \ell x_{\mathrm{c}}/l_{\mathrm{c}}$
ST Wall	Ω	$F_z \sim \eta r\Omega \varepsilon^{-1} L$	$\Delta \sim \sqrt{r/\delta}\ell$
Janus	Ω	$F_z \sim \eta r\Omega \varepsilon^{-1} L$	$\Delta \sim \ell\sqrt{r/\delta} - \dfrac{\ell\sqrt{r/\delta}}{\sqrt{1+\ell r^{1/2}\delta^{-3/2}}}$

4(a) shows the pressure distribution for the scenario of a moving cylinder over an inhomogeneous wall (trajectory shown in Fig. 1c). The no-slip solution maintains an anti-symmetric pressure distribution (red line). The introduction of a finite slip length breaks this symmetry (blue and black lines), as the gap pressure necessary to accelerate the flow through the gap (with varying thickness) is increased over the slippery section ($X < 0$). Figure 4(b) shows the gap pressure of the wall-parallel moving Janus particle (trajectory in Fig. 1d). Here, the induced lubrication pressure needs to accommodate both varying gap thickness and varying fluid shear in the gap, which results in a pressure peak also over slippery sections of the Janus cylinder. Note that due to the symmetry between the two configurations the pressure distributions in (a) and (b) are the mirror of distributions (c) and (d), respectively.

We now return to the examples reported in Fig. 2 to explain their trajectories using the components of the resistance matrix shown in Fig. 3. The oscillatory trajectory in Fig. 2(a) can be explained as follows. A slip-to-no-slip transition pushes the cylinder away from the wall (Fig. 1c), whereas a no-slip-to-slip transition produces a negative F_z, pulling the cylinder towards the wall. The long-term net migration away from the wall (Fig. 2a,ii) is partially because the push force is slightly larger than the pull force for each period due to different gap thicknesses during the pull and push events (see SI for an analysis).

The second example involves a rotating neutrally buoyant cylinder (Fig. 2b). When the cylinder is released

above a slippage transition on the neighbouring wall, we observe a migration in both $x-$ and z-directions (see Fig. 2b,ii). The resistance coefficients in Fig. 3(b) and (c) explain this behavior. The imposed rotation produces a wall-normal lift force ($F_z \sim \eta r\Omega f_z^{\omega} > 0$) and a negative transverse thrust ($F_x \sim -\eta r\Omega f_x^{\omega} < 0$). However, as the cylinder migrates away from the wall, we have $V^{\perp} > 0$, which leads to a positive transverse thrust ($F_x \sim \eta V^{\perp} f_x^{\perp} > 0$). The $V^{\perp}$-generated thrust dominates over the Ω-generated thrust, such that the cylinder moves in the positive x direction.

The final example involves a rotating neutrally buoyant Janus cylinder (Fig. 2c). The cylinder undergoes a spiralling motion that results in positive transverse propulsion and positive wall-normal migration. We may explain the spiral motion in the stages A-E depicted in Fig. 2(c). In stage A, the cylinder migrates upward since $\hat{f}_z^{\omega} > 0$. It simultaneously migrates to the left since, due to the short exposure, $V^{\perp}$ is relatively small and we have $|V^{\perp}\hat{f}_x^{\perp}| < |r\Omega\hat{f}_x^{\omega}|$. In stage B, the Janus cylinder has rotated sufficiently such that there is no more slippage in the gap. Therefore, a lift force is no longer generated and the wall-normal drag force $\hat{f}_z^{\perp}$ hinders further upward migration. Stages C and D are the mirror of A and B, respectively. Consequently, we observe a migration in the negative z and positive x directions. As the cylinder reaches stage E, it has experienced a net translation in the positive x direction and a small net migration away from the wall from its initial position A. This is due to the difference in the magnitude of fluid stresses in the gap when slip (B) and no slip (D) surfaces face the wall.

Finally, we turn to scaling analysis to estimate the induced lift force and the associated normal displacement. We focus on the instant where a cylinder is located right above the transition from slip to no slip on the neighbouring wall (Fig. 1a). Assuming no rotation and constant transverse velocity $V^{\parallel}$, a force balance (per unit length) in the wall-normal direction yields $\eta f_z^{\parallel} V^{\parallel} = \eta f_z^{\perp} V^{\perp}$, where the left and right-hand sides correspond to the magnitude of the lift and drag components, respectively. By carrying out an expansion in $L \ll 1$ of $f_z^{\parallel}$ and $f_z^{\perp}$ (see SI), we can approximate the two components, at lowest order in L, as

$$f_z^{\parallel} \simeq 4\ell r/\delta_0^2 \quad \text{and} \quad f_z^{\perp} \simeq -3\sqrt{2}\pi\left(\delta_0/r\right)^{-3/2}. \tag{8}$$

By assuming that the lift force approximately acts over the lubrication contact length l_c, we have

$$V^{\parallel} = l_c/\tau \qquad \text{and} \qquad V^{\perp} = \Delta/\tau, \qquad (9)$$

where τ is the time it takes to traverse l_c, and Δ is the displacement away from the wall. Inserting these estimates in the wall-normal force balance yields $\Delta \sim \ell$. This is in agreement with numerical results shown Fig. 1(c), where we observe $\Delta \approx \delta_0$ for $\ell \approx \delta_0$. Note that this leading order scaling estimate predicts no net displacement for particle travelling over two consequent transitions. To explain the net migration for the patterned wall (Fig. 2a), we modify the length over which the lift force acts (9) in an appropriate way (see SI). For a Janus cylinder (Fig. 1b), there is no fixed time over which the displacement occurs, because the transition point travels along with the cylinder. Therefore, we expect a displacement $\sim \ell$ for each l_c traversed. This yields the estimate,

$$\Delta \sim \ell x_c/l_c, \qquad (10)$$

where x_c is the distance traversed along the wall. Table I, summarizes the scaling estimates of the lift force and normal displacement, induced by transverse motion or rotation, for both systems in Fig. 1(a,b) (see SI).

To conclude, we have used a combination of numerical simulations, analytical results obtained from lubrication theory, and scaling arguments, to describe how fluid-immersed objects approaching contact with spatially inhomogenous slippage properties may trigger novel nontrivial forces and torques. We have further shown how striking and active-like particle trajectories can emerge as a consequence. This opens up new interesting opportunities for the design of interfaces to control and influence nearby particle motion, as well as to reduce friction and wear. It also provides a foundation to explore more complex particles and interfaces in order to understand fundamentally more realistic situations found in nature and especially biology.

[1] O. Reynolds, Philos. Trans. R. Soc. London **177** (1886).

[2] D. Jeffery and Y. Onishi, Q. J. Mech. Appl. Math. **34**, 129 (1981).

[3] B. Rallabandi, N. Oppenheimer, M. Y. B. Zion, and H. A. Stone, Nature Physics **14**, 1211 (2018).

[4] K. Sekimoto and L. Leibler, EPL **23**, 113 (1993).

[5] J. M. Skotheim and L. Mahadevan, Phys. Rev. Lett. **92**, 245509 (2004).

[6] B. Saintyves, T. Jules, T. Salez, and L. Mahadevan, P. Natl. Acad. Sci. USA **113**, 5847 (2016).

[7] T. Salez and L. Mahadevan, J. Fluid Mech. **779**, 181196 (2015).

[8] B. Rallabandi, B. Saintyves, T. Jules, T. Salez, C. Schönecker, L. Mahadevan, and H. A. Stone, Phys. Rev. Fluids **2**, 074102 (2017).

[9] A. Steinberger, C. Cottin-Bizonne, P. Kleimann, and E. Charlaix, Phys. Rev. Lett. **100**, 134501 (2008).

[10] S. Leroy, A. Steinberger, C. Cottin-Bizonne, F. Restagno, L. Léger, and E. Charlaix, Phys. Rev. Lett. **108**, 264501 (2012).

[11] J. Yan, M. Bloom, S. Bae, E. Luijten, and S. Granick, Nature **491**, 578 (2012).

[12] R. Golestanian, T. B. Liverpool, and A. Ajdari, Phys. Rev. Lett. **94**, 220801 (2005).

[13] J. S. Wexler, A. Grosskopf, M. Chow, Y. Fan, I. Jacobi, and H. A. Stone, Soft Matter **11**, 5023 (2015).

[14] D. Attinger, C. Frankiewicz, A. R. Betz, T. M. Schutzius, R. Ganguly, A. Das, C.-J. Kim, and C. M. Megaridis, MRS Energy & Sustainability **1**, E4 (2014).

[15] E. Lauga, M. Brenner, and H. Stone, Springer handbook of experimental fluid mechanics , 1219 (2007).

[16] L. Bocquet and J.-L. Barrat, Soft Matter **3**, 685 (2007).

[17] U. Lacis and S. Bagheri, J. Fluid Mech. **812**, 866889 (2017).

[18] J. P. Rothstein, Ann. Rev. Fluid Mech. **42**, 89 (2010).

[19] T.-S. Wong, S. H. Kang, S. K. Y. Tang, E. J. Smythe, B. D. Hatton, A. Grinthal, and J. Aizenberg, Nature **477**, 443 (2011).

[20] J. L. Anderson, Ann. Rev. Fluid Mech. **21**, 61 (1989).

[21] U. Kaynan and E. Yariv, Phys. Rev. Fluids **2**, 104103 (2017).

[22] Typical parameters are: red blood cell radius $r = 3\,\mu\text{m}$, cell-wall gap $\delta = 0.5\,\mu\text{m}$, fluid viscosity $\eta = 1.5\,\text{mPa}\,\text{s}$, and speed $V^{\parallel} = 0.286\,\text{mm}\,\text{s}^{-1}$ estimated by multiplying the $100\,\text{s}^{-1}$ shear rate and the cell radius [23].

[23] H. S. Davies, D. Débarre, N. El Amri, C. Verdier, R. P. Richter, and L. Bureau, Phys. Rev. Lett. **120**, 198001 (2018).

[24] L. G. Leal, *Advanced transport phenomena: fluid mechanics and convective transport processes*, Vol. 7 (Cambridge University Press, 2007).